THE ISOCAM CVF CALIBRATION REPORT

A. Biviano[1,2], B. Altieri[1], J. Blommaert[1], F. Boulanger[3]
D. Cesarsky[3], L. Metcalfe[1], K. Okumura[1], W. Reach[3,4]

1: CAM IDT, ESA Satellite Tracking Station, PO Box 50727, E-28080 Madrid, Spain
2: Osservatorio Astronomico di Trieste, via G.B. Tiepolo 11, I-34131 Trieste, Italy
3: IAS, Université Paris XI, Bât.121, F-91405 Orsay, France
4: California Institute of Technology, IPAC, MS 100-22, Pasadena, CA 91125, USA

Version 1.1 – May 20^{th}, 1998

Abstract

We present here the current status of calibration of the Circular Variable Filters (CVF) of the ISO-CAM instrument. Specifically, we address the topics of the Spectral Response Function (SRF hereafter), of spectral purity (i.e. the wavelength calibration), and of ghost images and straylight.

CVF photometry on a single star is shown to be repeatable at a level of ~ 3 %. The RMS uncertainty on the SRF, calibrated using several stars, is also ~ 3 %.

There are two kinds of ghosts in the CVF images, one comoving with the source image, the other moving symmetrically with respect to the array center. Preliminary estimates of the ghost photometry and spectra are given, as well as indications of how the straylight affects the image of an uniform background, leading to characteristic features in the CVF flat fields.

For what concerns the spectral purity, the measured spectral lines of several sources are shown to fall into the expected CVF step positions, when the image of the source is centered in the middle of the array. When the source image is at the edge of the array, there is a wavelength shift that depends on the wavelength itself, and may go up to 0.1 μm.

1 Introduction

Spectroscopy with ISO-CAM means observing with the Circular Variable Filters (CVF hereafter). We refer the reader to the "ISOCAM Observer's Manual" for a full description of the CVF.

The CVF covers the wavelength range from 2.273 μm to 16.52 μm with three segments, one in the SW channel of CAM and two in the LW channel, using 274 step positions. However, there are some step positions outside this range that are not recommended for use.

The advantage of using the CVF is that it allows spectro-imagery with a high sensitivity. On the other hand, the resolution is limited to about $\lambda/\delta\lambda \simeq 40$.

In this paper, we describe the current status of the CVF calibration, as obtained "in-orbit" from dedicated calibration observations. In § 2 we give an overview of the data taken for calibration purposes and describe the data-reduction; in § 3 we describe the calibration of the spectral response function (SRF hereafter); in § 4 we describe our current understanding of the properties of the ghost images and straylight that affect CVF observations; in § 5 we deal with the wavelength calibration of the CVF, the so-called "spectral purity". We give our conclusions in § 6.

2 The calibration data

The main calibration topics for CVF are:

- spectral response function;
- wavelength calibration;
- ghost/straylight;
- cross-calibration (with CAM filters and other ISO instruments).

For what concerns the SRF calibration, several stars have been observed, spanning 2 orders of magnitude in brightness range. In the PV-phase, three stars were observed, HIC94890, HIC96441, and HIC94376 (δ Draconis). In the routine phase, the main calibrating stars have been HIC94376 for the LW CVF1 and CVF2, and HIC96441 for the SW CVF. For reasons of time, it was not always possible to cover all steps of all CVF segments, nor to always perform double-scan observations (from short to long wavelengths and back), although this strategy helps to minimize transient problems. More often, the $3''$ pixel-field-of-view (PFOV) has been used, but also $1.5''$ and $6''$PFOV observations have been done in order to check the photometry.

While the highest wavelength step of the CVF is nominally 16.52 μm (see "The ISOCAM User's Manual") additional steps exist. An attempt has been made to calibrate the CVF SRF up to 17.34 μ, via the observation of the very bright star δ Draconis (the sensitivity of the CVF at these extreme step positions is very low).

The wavelength calibration has been based on the observations of planetary nebulæ with known strong lines. Two planetary nebulæ (NGC6543 and NGC7027) were observed in the PV-phase, and the Helix nebula in routine phase.

Ghost and straylight calibration were done using observations of both point and extended sources. In particular, the star HIC94376 has been observed several times in different positions of the detector, and at different CVF steps, to characterize the ghost image flux and position. The zodiacal background has also been observed at different PFOVs and different CVF step positions to characterize the straylight pattern on the final CVF images.

Two very bright stars (γ Draconis and Sirius) and several solar-system objects (Neptune, Cybele and Hygiea) have been observed with the purpose of cross-calibration with other ISO instruments. In general, the brightness of these objects is too high for allowing observation through all CVF segments (e.g. the two stars are too bright at short wavelengths, so that they could not be observed with the SW CVF, nor at all steps of the LW CVF1). Other observations were done with the purpose of cross-calibrating the CAM filters and the CVF, on red-spectrum stars, extended sources (like active galaxies), and asteroids.

The integration times used were typically 2.1 or 0.28 seconds. As there are many step positions per each CVF segment, one must choose short integration times in order to have a sufficient number of frames per CVF step position (~ 20) so to allow a proper deglitching.

The data-reduction is standard: after subtracting the dark current, using the available CAL-G dark, or the time-dependent dark-current model of Biviano et al. (1998), the data cube is cleaned from glitches, using the CIA (Ott et al. 1996, Delaney 1997) algorithms *TCOR, TEMP* or *MM*. Note that the jitter of the ISO pointing moves the centre of the star image from one frame to another; this causes a high-frequency change in the brightness of the two or three pixels that see the peak of the star point-spread-function (PSF hereafter). Some deglitching algorithm may misinterpret this jitter-induced rapid change of brightness of the central pixels as due to glitches, with terrible consequences for the photometry. Special care has been devoted to choose the deglitching method in such a way as to avoid this problem.

After deglitching, in some cases the IAS transient correction routine has been applied (Abergel et al. 1996), or, before this routine became available, the standard CIA *S90* routine. Note that there are not generally enough frames per CVF step position to allow the application of the *KSIG* routine (which is very widely used for many other observational data).

Afterwards, the individual frames of each CVF step position are averaged together, masking out those pixels affected by glitches or those frames that were used for initial stabilization, and finally the images are flat-fielded using the nearest-wavelength filter flat-field (CVF flat-fields cannot be used, since they are affected by straylight; see § 4.2).

3 The spectral response function

3.1 Analysis

The SRFs have been measured using all available data on photometric stars. The measurement of the flux of a point-source on the CAM detector is relatively straightforward.

The photometry of the stars was done following the method of Blommaert (1998), for ensuring consistency between the filter photometry and the CVF photometry.

For what concerns the SW detector, only one star was used for computing the SRF, i.e. HIC96441, for which four CVF scan observations were available. For what concerns the LW detector, several observations of four stars, HIC94890, HIC96441, HIC94376, and HIC87833 were used for computing the SRF.

For the SW observations, the star flux was computed within circles of 8, 6, and 4 pixel radii, at 1.5$''$, 3$''$ and 6$''$PFOV, respectively, with a background determined within an annulus 2-pixel wide, separated by one pixel from the inner circle (except in the case of the 1.5$''$PFOV, in which case a separation of two pixels was used). This flux-estimate is a good approximation to the total flux of the star, since the PSF width at short wavelengths is small.

For the LW observations, the star fluxes were computed within circles of 6, 4, and 2 pixel radii, at 1.5$''$, 3$''$and 6$''$PFOV, respectively, with a background estimated within annuli 2, 2, and 1 pixel wide, at 1.5$''$, 3$''$, 6$''$PFOV, respectively, separated by one pixel from the inner circle. In this case, these background-subtracted aperture fluxes had to be corrected using a theoretical PSF (Okumura 1998a), that was scaled according to the PFOV and the wavelength.

These total fluxes in detector units were divided by the star fluxes (in Jy), as obtained from the Ground Based Preparatory Program (see, e.g., Blommaert 1998) for the star HIC94890, and from Cohen et al. (1995; see also *The Calibration Liaison Web Page,* at http://isou24.vilspa.esa.es:888/) for the other three stars.

A weighted average of all the resulting SRF-estimates was done, by taking care not to include measurements strongly affected by transient effects.

The final SRFs were smoothed using a 3-pole digital low-pass filter, with a cut-off at 25 %, in order to reduced the noise features (that could be misinterpreted as spectral lines when the SRF is used to derive the spectrum of a given object).

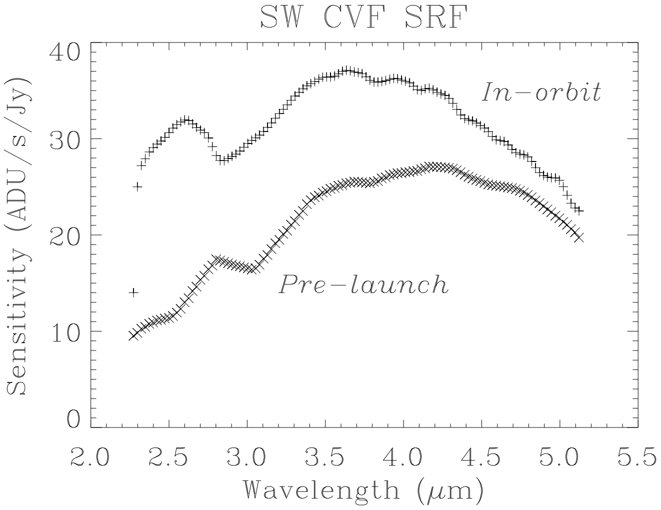

Figure 1: The pre-launch and in-orbit estimates of the SW CVF SRF (X's and crosses, respectively).

3.2 Results

3.2.1 Comparison with pre-launch estimates

In Fig.1 and 2 we have plotted the SRFs of the SW and, respectively, the LW CVFs (note that the two segments of the LW CVF are plotted together). In these figures we show both the pre-launch estimates of the SRFs and the current estimates of the SRFs, in units of ADU/s/Jy (an ADU[1] is the Analog-to-Digital Unit of ISO-CAM).

It can be seen that the SW CVF SRF has a higher sensitivity than expected from pre-launch measurements. It is 3 times more sensitive at short wavelengths and approximately as sensitive at long wavelengths. The *shape* of the pre-launch SW SRF is very different from the one measured in-orbit. The reason for that has been found to lie in an error in the pre-launch SRF (M. Perault, private communication; this is also true for the SW filter sensitivities, see Blommaert 1998). More specifically, the error consisted in neglecting an inverse λ dependence. If the pre-launch SRF is multiplied by $5.5/\lambda$, the agreement with the in-orbit SRF is greatly improved, and the two SRFs differ on average by $\simeq 1$ %. The difference is within ± 7 % for all positions at $\lambda > 3$ μm, but it is larger (up to 60 %) for positions at shorter wavelengths.

Contrarily to the trend seen for the SW CVF SRF, the LW CVF SRF has a lower sensitivity than expected from pre-launch measurements. The LW CVF SRF is 0.8 the pre-launch estimation, on average, but differences larger than 100 % are seen at some step positions (especially at the short-wavelength edge of the CVF2 segment).

We believe that the ~ 20 % difference between the in-orbit and pre-launch estimations of the LW CVF SRF may come from the difference between the PSF observed through the CVF, and the theoretical PSF we used for photometry. Indeed, the observational PSF include a ghost image of the star that contains ~ 20 % of the total flux (see § 4 and Okumura 1998a). The LW CVF SRF should in principle be derived using the observed PSF, but it cannot be done before an accurate characterisation of the ghost images is done (see Okumura

[1] CVF observations are sometimes done with a gain factor $\times 1$, and sometimes with a gain factor $\times 2$. Here and in the rest of this document, all units are scaled by the gain factor *even if not explicitely indicated* – i.e. both "ADU" and "ADU/G" mean Analog-to-Digital Units scaled by the gain factor.

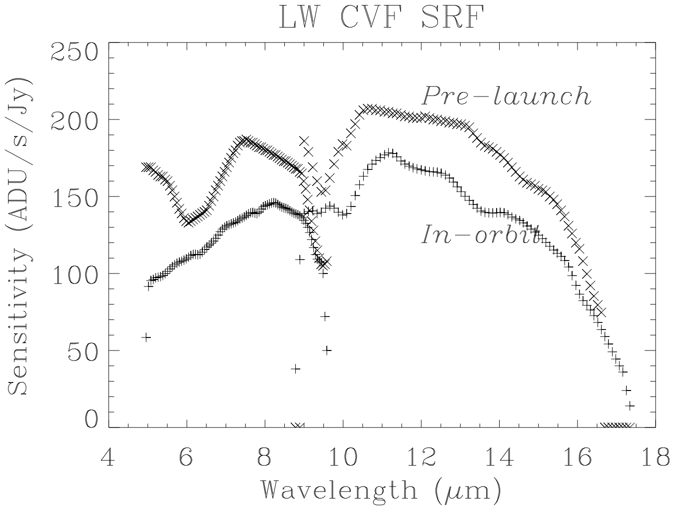

Figure 2: The pre-launch and in-orbit estimates of the LW CVF SRF (X's and crosses, respectively). Both segments of the LW CVF (CVF1 and CVF2) are shown.

1998b). Moreover, using the theoretical PSF ensures consistency with the photometry done with the wide-band filters (Blommaert 1998). However, we caution the observer that CVF observations, mostly those at 6″PFOV, are affected by ghost images, whose flux must not be included when transformation from detector to physical units is done using the SRF we have derived (see also § 4.1.1).

Note that there are a few positions at wavelength $\lambda \geq 16.52$ that are outside the recommended range for use (see "The ISOCAM Observer's Manual"), and were not included in the pre-launch SRF estimation. The SRF of these CVF positions has been calibrated during the ISO mission for completeness.

3.2.2 Accuracy of the SRF estimation

The repeatibility of the CVF photometry *on the same star* is excellent, ± 3 % rms. On the other hand, it is wiser to use more than one star for deriving the SRF, in order to check that the SRF is the same for different flux levels, and to minimize possible systematic errors in the models to which our observations are confronted. The RMS is likely to be a little bit larger when more than a single star are considered.

The error bars of the derived CVF SRFs are shown in Fig. 3 (SW CVF), Fig. 4 (LW CVF1) and Fig. 5 (LW CVF2), along with the SRFs themselves. These error bars represent the RMS of different measurements used for deriving the SRFs, and do not include any systematic errors, such as those coming from the presence of ghosts (see § 4). The average random error of the SW CVF SRF is ~ 3 %, but in some SW CVF positions the error is as large as 23 %.

The RMS of the LW CVF1 SRF is 3 %, on average, and always < 17 %, except for the very last CVF step position at long wavelength, where the RMS is ~ 60 % of the measured value. Fortunately, the same wavelength is also covered by the LW CVF2, with a much better accuracy. Overall, the RMS of the CVF2 SRF is 4 %, on average, and < 18 % at all CVF positions normally available to the observer, i.e. from 9.003 to 16.52 μm (see the "ISOCAM Observer's Manual"). The SRF at CVF positions outside the recommended range is affected by much larger errors (average of 20 % and up to 100 %).

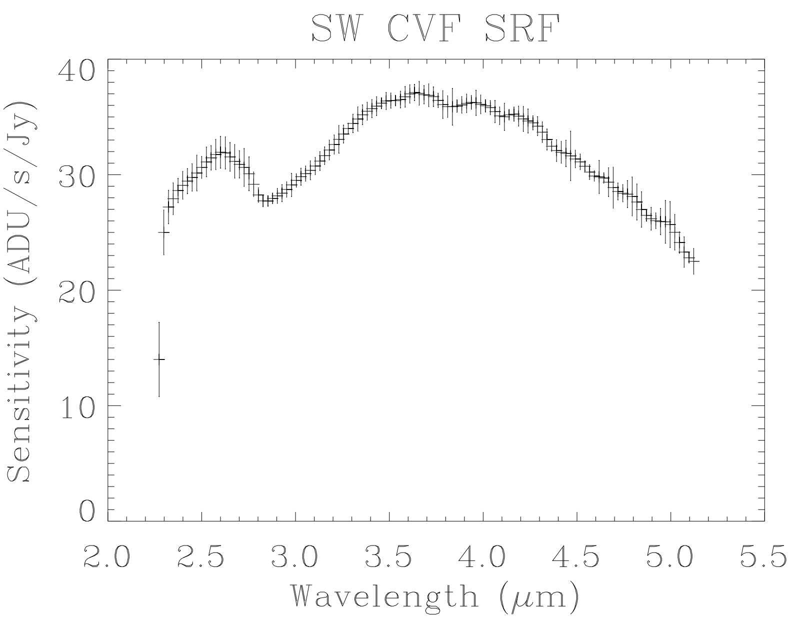

Figure 3: The SW CVF SRF within its $\pm 1\sigma$ confidence band (shaded region), where σ is the RMS obtained from the several measurements used to obtain the SRF.

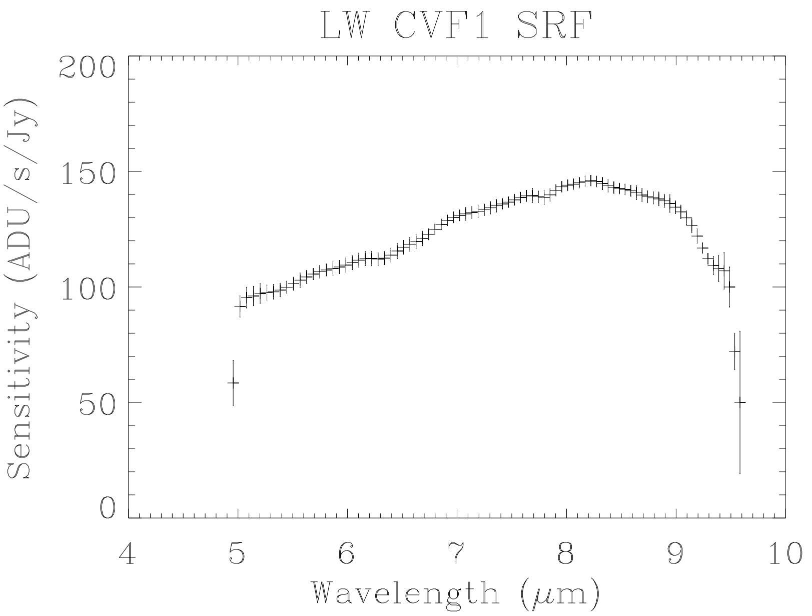

Figure 4: The LW CVF1 SRF within its $\pm 1\sigma$ confidence band (shaded region), where σ is the RMS obtained from the several measurements used to obtain the SRF.

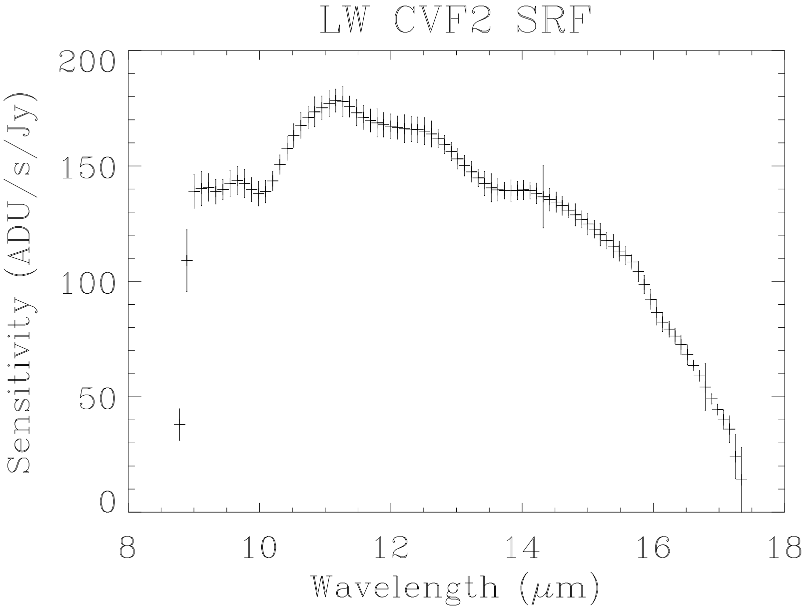

Figure 5: The LW CVF2 SRF within its $\pm 1\sigma$ confidence band range (shaded region), where σ is the RMS obtained from the several measurements used to obtain the SRF. Note that the use of the CVF2 positions at $\lambda < 9.003\mu m$ and $\lambda > 16.52\mu m$ is not recommended.

3.2.3 Effects of stabilization

Part of the scatter in the CVF SRF comes from incomplete stabilization. The CVF scan observations are very time consuming and it is not possible to spend more than ~ 20 frames per position within the available calibration time (as an example, a full scan of the SW CVF at 2 sec integration time with 20 frames per position requires 1.3 hours).

In Fig. 6 we show the signal time histories of the brightest pixel of the HIC96441 star image, observed at the first SW CVF position at the beginning and at the end of a forth+back scan. Stabilizing trends can clearly be seen. When the star is observed the first time at the first CVF scan position, an upwards stabilizing behaviour can be seen, due to the fact that the pixel signal is stabilizing from a low to a high flux level. A hundred frames were spent on this first position, with the purpose of allowing a stabilized signal to be reached. However, all following CVF steps were done with only 20 frames, for 100 frames per step would have been too much time consuming. The consequence of this (forced) choice is the incomplete downward stabilizing trend of the same pixel signal when the same star is observed again at the same CVF position, at the end of the backward scan, started after the forward scan (from short to long wavelengths) was completed. The downward stabilizing trend is due to the fact that a higher flux was falling onto that pixel in the previous position, because the CVF is much less sensitive at the first position than at the second one while the star flux is similar. It is clear that stabilization is not achieved yet, and, more importantly, the two observations do not converge to the same signal. The *total* flux derived for the star at this CVF position was 238 ADU/s on the forward scan, but much higher (404 ADU/s) on the backward scan.

Currently available models for transient-correction can however help to improve the situation. An example of this is shown in Fig. 7, where we plot the fluxes of the star HIC96441 obtained in two consecutive CVF2 scans (forward and backward), before and after the transient correction developed by Abergel et al. was applied. The relatively large flux differences

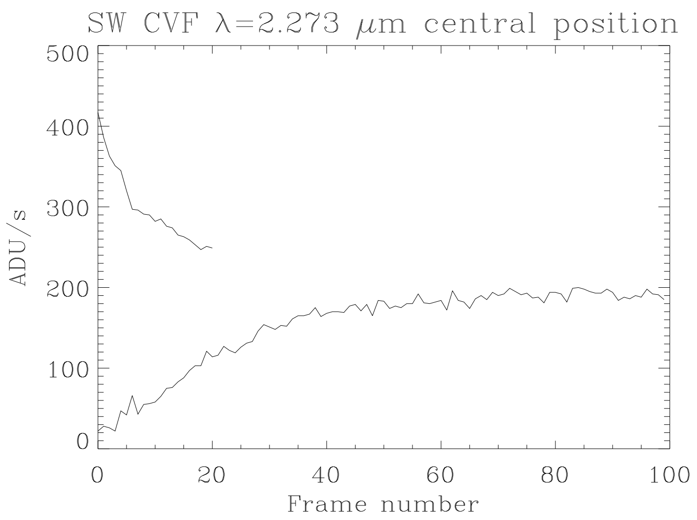

Figure 6: The signal time histories of the brightest pixel of the HIC96441 star image, at the first SW CVF position, observed during a forward (short to long wavelengths) scan, and a following backward scan. The first time the pixel sees the star, during the forward scan, the signal is stabilizing upwards and is possibly stabilized after $\sim$ 100 frames; the second time, there is a downward stabilizing trend but the observation is too short to allow reaching complete stabilization.

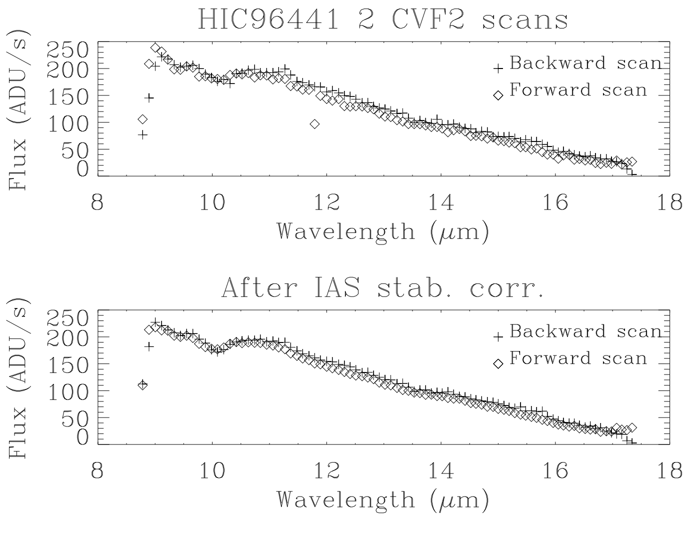

Figure 7: The spectrum of the star HIC96441 observed twice, once in a forward scan from short to long wavelengths, and immediately after in a backward scan. The top panel shows the spectrum obtained without any transient correction. The bottom panel shows the spectrum derived using Abergel et al.'s transient correction.

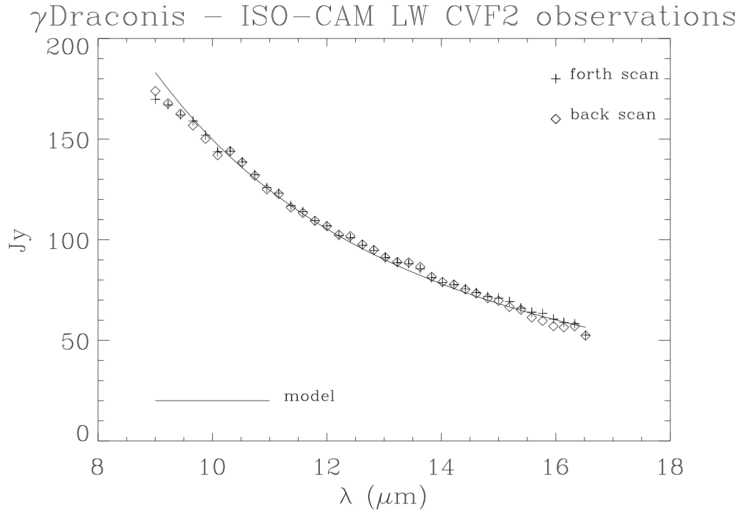

Figure 8: The spectrum of the star γ Draconis observed twice with the LW CVF2, once in a forward scan from short to long wavelengths, and immediately after in a backward scan. The line shows a composite spectrum derived from non-ISO observations by Cohen et al. (1995).

between the forth and the back scans are diminished, and overall the star spectrum looks less noisy, after the transient correction is applied. Note however that observations of our primary calibrating star, HIC94376, suffer much less from transient effects, because its flux is much higher than the flux of HIC96441 (more than a factor 10).

We have not yet applied a transient correction model to all our calibration observations, because the model is still being refined. However, the examples given above show that our current understanding of the transient behaviour of CAM pixels is good, and we expect to further improve upon this topic in the near future, possibly by using new techniques (e.g. Lari 1997).

3.3 Absolute flux calibration: γ Draconis

The very bright star HIC87833, or γ Draconis, has been observed with CVF2 in rev.482, for the purpose of cross-calibration with other ISO instruments (PHT and SWS) and for a comparison with a composite spectrum assembled from ground-based and KAO observations (Cohen et al. 1995), data from the IRAS Point Source Catalogue and an IRAS Low Resolution Spectrum. Here we quote results of the comparison of our CAM observations with the composite spectrum from Cohen et al.

In Fig. 8 we show the spectrum of this star (in Jy) as obtained through two consecutive forward and backward scans, as compared with Cohen's composite spectrum. Note that this spectrum was derived with an early version of the CVF SRF, that was *not* based on observations of this same star. It can be seen that the CAM spectrum agrees with the composite spectrum over all the range of observed wavelengths (9 to 16.5 μm); there is no average systematic deviation and the RMS deviation is only 2 %. This is fully consistent with the accuracy derived for the CVF2 SRF.

The good results of this cross-correlation pushed us to include the CVF observations of this star into the data-base for derivation of the CVF2 SRF.

4 Ghosts and straylight

Ghost-images and straylight are important in CVF. This was expected since, at variance with CAM filters, the CVF could not be tilted with respect to the optical axis. The presence of ghost-images and straylight affects photometry and imaging.

4.1 Ghost images from point-scources

In Fig. 9 I have plotted three independent observations of the same star, δ Draconis, done with CVF at $6''$PFOV, at a wavelength $\lambda = 7.358\mu$m (the intensity scale is logarithmic). In one of the observations, the star image is at the centre of the array, in the other two, it is at the left and right edges. Two types of ghost-images can be seen. One has a ring-shape and is comoving with the source image. The other has a circular shape and moves symmetrically with respect to the CAM array centre, as the source moves.

While not shown in the figure, the ghost images have similar features (but different relative intensities) at different wavelengths[2].

I will call the two kinds of ghost the *comoving* ghost and the *symmetric* ghost, respectively.

The results of aperture photometry on the source and the ghost images are shown in Fig.10 and Fig.11 for the CVF1 and, respectively, the CVF2. We can notice that the *comoving* ghost spectrum looks similar to the source spectrum, except maybe at the short-wavelength edge of the CVF1, and at the long-wavelength edge of the CVF2. The *symmetric* ghost spectrum seems significantly different from the source spectrum at long wavelengths with the CVF2. It is noticeable that the spectra measured for the *symmetric* ghost, on the left and on the right offset positions, are almost identical.

Since most of the differences between the star and the ghost spectra are seen at extreme CVF positions, it is possible that these differences are only due to a poor stabilization of the ghost images (the image of the star stabilizes faster since it is brighter). It is therefore too early to conclude that the source and ghost spectra are indeed different.

The ratio between the ghost and the star flux is ~ 20 %, on average, for the *comoving* ghost, and only ~ 4 % for the *symmetric* ghost. The ~ 20 % flux lacking can account for the difference between the pre-launch and the in-orbit estimations of the SRF (see § 3.2.1).

4.1.1 Photometry with different pixel field-of-views

The ghosts are clearly seen in the images taken at $6.0''$PFOV. However, the distance of the ghost-images from the direct images of the source is such that neither the *symmetric* nor the *comoving* ghost can be seen at smaller PFOVs. In such a case, part of the source flux (i.e. that part that is usually seen in the ghost at $6.0''$PFOV) is lost. As a consequence, aperture photometry on a source observed at $6.0''$ may give different results from aperture photometry on the *same* source at a smaller PFOV ($3.0''$ and $1.5''$), if the aperture is chosen large enough to include the ghost images at $6''$PFOV.

This point is illustrated in Fig.12. In the figure I have plotted the aperture flux of the star δ Draconis, at $\lambda = 6.511\mu$m as measured within a circle of given radius, with three different PFOVs. Two arrows are shown, indicating the inner and outer radius of the region where the *comoving* ghost can be seen on the image. The same physical aperture radius corresponds to different aperture radii, in pixels, for different PFOVs, and it is two (four) times larger at $3.0''$ ($6.0''$) than at $1.5''$. The small difference in the fluxes measured at $1.5''$ and $3.0''$PFOV is due to the fact that the background is estimated closer to the source in the $1.5''$PFOV image than in the $3.0''$PFOV image. On the other hand, the difference in the fluxes measured at $3.0''$and $6.0''$PFOV is larger, and due to the contribution of the

[2] The interested reader may find other images/movies of these ghosts on the web, at http://isowww.estec.esa.nl/instr/CAM/cvf_ghst.html

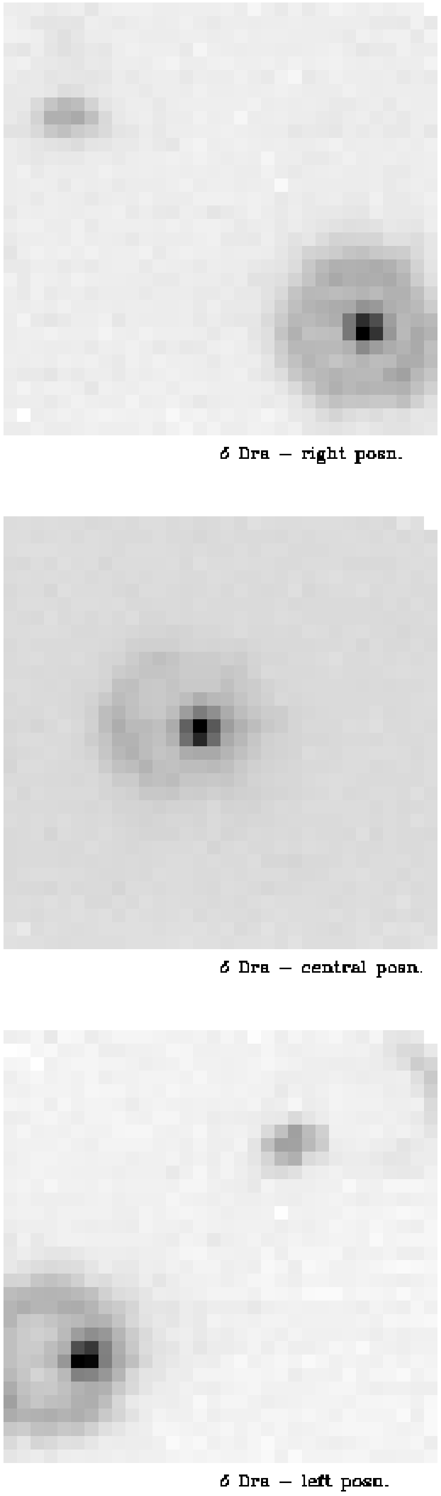

Figure 9: Ghost images in three CVF observations of δ Draconis. Intensity scales are logarithmic.

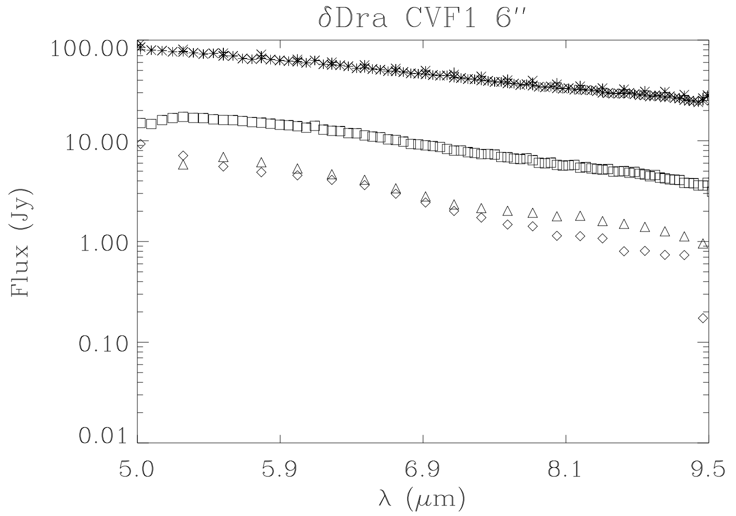

Figure 10: Aperture photometry on the star δ Draconis and its ghost images with the CVF1. Asterisks, pluses, and X's indicate three independent measurements of the star fluxes; squares indicate measurements of the *comoving* ghost fluxes; triangles and diamonds indicate measurements of the *symmetric* ghost fluxes, at the left and the right off-centre positions, respectively. Scales are logarithmic.

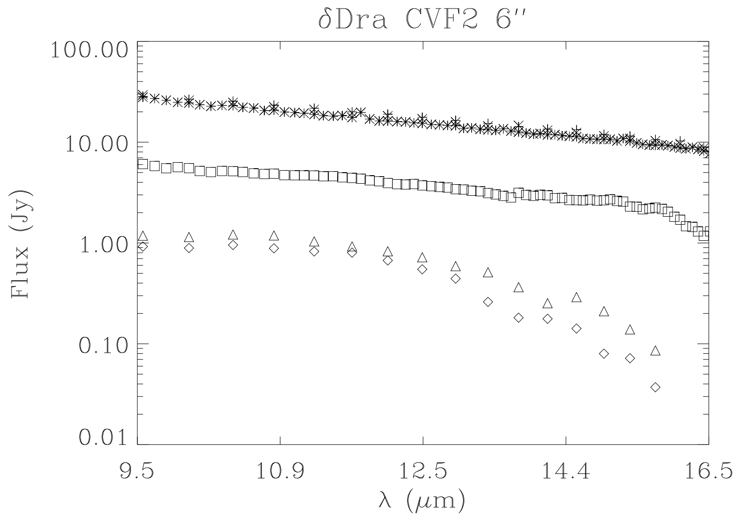

Figure 11: Aperture photometry on the star δ Draconis and its ghost images with the CVF2. Symbols are the same of Fig. 10. Scales are logarithmic.

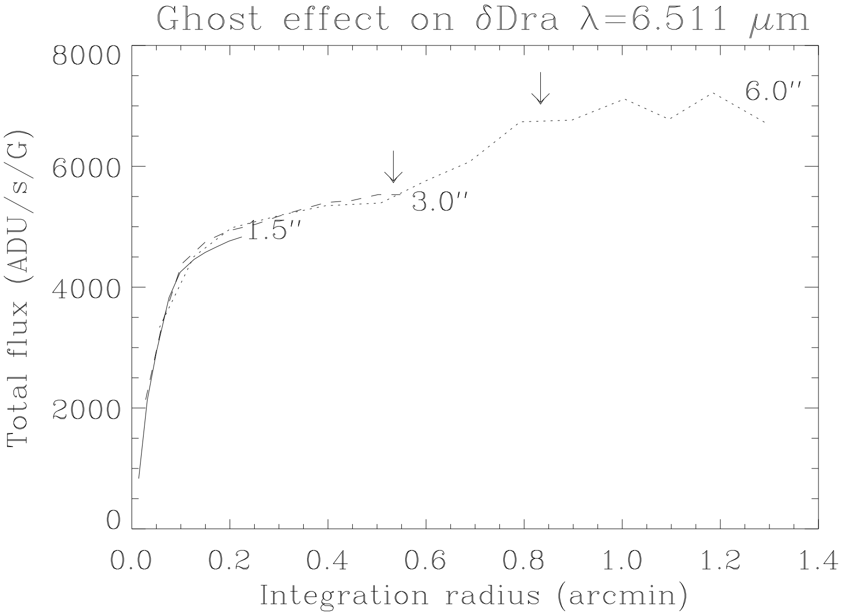

Figure 12: Aperture photometry on the star δ Draconis at $\lambda = 6.511\mu$m and at three different PFOVs (indicated). The arrows indicate the inner and outer radius of the region where the *comoving* ghost can be visually identified on the image.

ghost. In fact, the integrated flux reaches a first *plateau* at an aperture radius corresponding to the distance of the ghost-image from the source-image ($\sim 0.55'$ in this case), then raises rapidly because of the flux contribution from the ghost, and then reaches a second *plateau* when all the ghost image is contained within the chosen aperture ($\sim 0.8'$ in this case).

It is clear that in order to avoid systematic errors in the CVF photometry one must be aware of the ghost flux contribution. Since the SRF has been derived without including the ghost flux into the estimation of the total flux from a star (see § 3), for consistency observers *should not include the ghost flux* in the estimation of the total flux of a given source (though we understand that the identification of ghost images may be difficult when the source is extended).

4.2 Straylight from extended sources

Straylight from extended sources was investigated through observations of zodiacal background regions with three CVF step positions (corresponding to the wavelengths of 7.7, 11.4 and 15 μm), and all PFOVs.

In Fig.13 we show the image obtained on the the zodiacal background at 11.4 μm with 12.0″PFOV, after the usual data-reduction (without flat-fielding). In this configuration, the field mirror acts as a field stop, and only the central 16×16 pixels of the detector array should be illuminated. However, one can see from the figure that the region of the detector not covered by the field-mirror is not dark, but illuminated by straylight. The total flux outside the field-mirror region sums up to ~ 25 % of the flux within the region covered by the field-mirror (see also Okumura 1998a).

In Fig.14 we show the image obtained on the zodiacal background at 11.4 μm with 6.0″PFOV, after the usual data-reduction, including flat-fielding (we have used the closest wavelength flat-field image available, i.e. that taken with the LW10 filter). Despite the

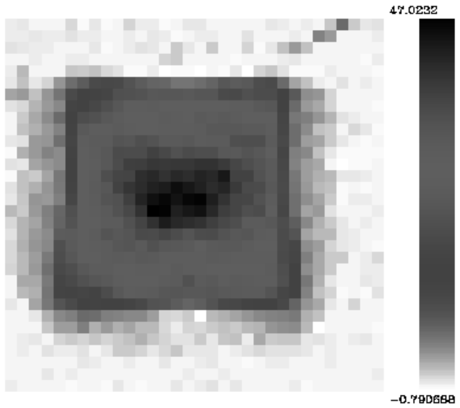

Figure 13: An image of the zodiacal background taken with the CVF at 11.4 μm, with 12.0″PFOV. Flux units are ADU/g/s.

image has been flat-fielded and the target is a flat sky region, significant structures can be seen. The deviation from flatness of this image can be quantified in terms of the RMS of all pixel fluxes relative to the median flux: 10 %. This means that, in a CVF image, real physical structures with an average per-pixel flux $\leq$ 10 % of the background, are hard to detect, unless this straylight effect is corrected. The characteristic double-lobe CVF flat-field pattern, visible in Fig.14, can indeed lead to misinterpretations of the CVF images (e.g. the straylight pattern could be incorrectly attributed to extended emission around a target star).

Of course, the situation gets worse when also bright sources (theoretically outside the field-of-view) contribute to the straylight.

It is therefore important to correct for this straylight effect. A possible way is to subtract from the scientific images these calibration images (available to all observers under the form of CAL-G files), after appropriate scaling for taking into account the background flux variations from one image to another. However, a detailed modelling of the CAM optics is needed to properly taking into account this effect (Okumura 1998b).

5 Spectral purity

From observations of planetary nebulæ taken during the PV-phase, the central wavelengths of two lines, NeII and SIV were derived (by simple gaussian fitting over the continuum). They were found to fall at the expected CVF positions, within a few hundreths of a CVF step. Transient effects may slightly change the observed position of the line, by less than a tenth of a CVF step.

The wavelength purity is reduced when the source is not centered at the middle of the array. An analysis of the NeIII-line central position in a CAM CVF image of M17 has shown that the central observed wavelength position of the NeIII line is 0.09 μm higher at the left edge of the CAM array than at the centre. At the position of the CVF2 corresponding to the wavelength of the NeIII line (15.555 μm), such a shift corresponds to roughly a CVF step. At the right edge, however, there is no significant wavelength shift.

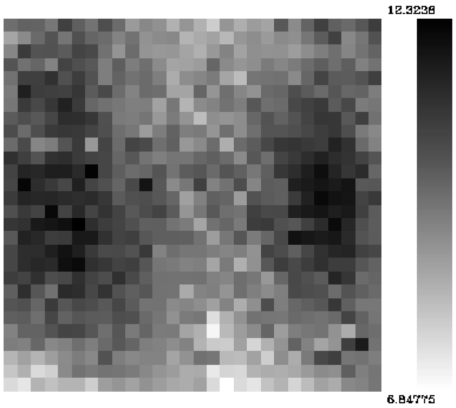

Figure 14: An image of the zodiacal background taken with the CVF at 11.4 μm, with 6.0″PFOV. Flux units are ADU/g/s.

On the other hand, there is no wavelength-dependence on the top-down direction of the array, as expected from the orientation of the CVF with respect to the array.

These results are confirmed by independent observations of the NGC 6543 planetary nebula, whose image was positioned on the left and right edges of the CAM detector. In Fig.15 and Fig.16 I show the spectrum of NGC 6543 as obtained with the CVF with the source image positioned at two CAM edge positions, around the wavelength of the ArIII line, and the NeII line, respectively. It is clear that when the source image is located on the right edge of the detector there is no significant wavelength shift, while when the source is located on the left edge of the detector, the shift is siginificant, and equal to 0.023 μm at the wavelength of the ArIII line, 8.991 μm, and to 0.109 μm at the wavelength of the NeII line, 12.814 μm. These results are consistent with those found for M17. In addition, there is an indication that the wavelength-shift is wavelength-dependent, being larger at longer wavelengths.

Further investigation is needed on this topic to achieve a full calibration of the CVF spectral purity. Currently available observations of extended sources will be used to map the wavelength-shift of the CVF observations over the CAM array.

6 Conclusions

The SRF of the CVF is currently well constrained, to within ± 3 % on average. The SRF has been obtained from the comparison of the total fluxes of several calibration stars and their models and/or ground-based observations. The total flux of a star has been derived from PSF-corrected aperture photometry. Since the *observed* PSF in several CVF positions is affected by the presence of ghost images, we preferred to use the theoretical PSF, scaled according to the wavelength and PFOV, for estrapolating the flux derived from aperture photometry to a total flux. Note that the derived fluxes do not include the flux associated with ghost images.

The flux contribution from ghost images of the target source is important, $\sim$ 20–25 % of

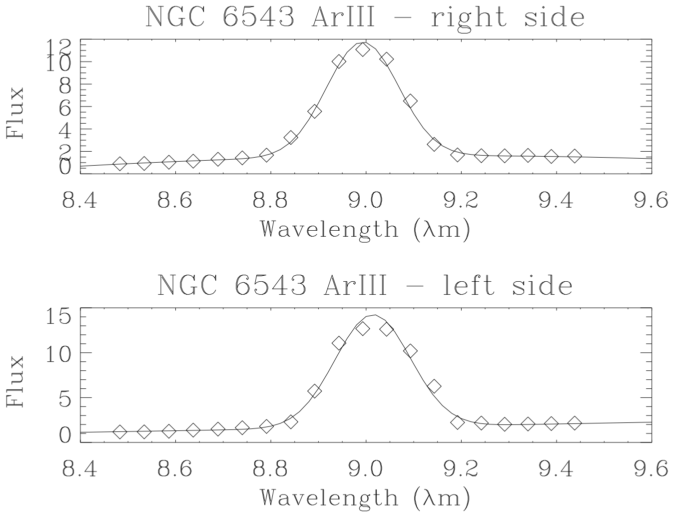

Figure 15: The spectrum of NGC 6543 around the ArIII line, as observed with the source put on the right side (top panel) and the left side (bottom panel) of the CAM detector. Flux units are arbitrary.

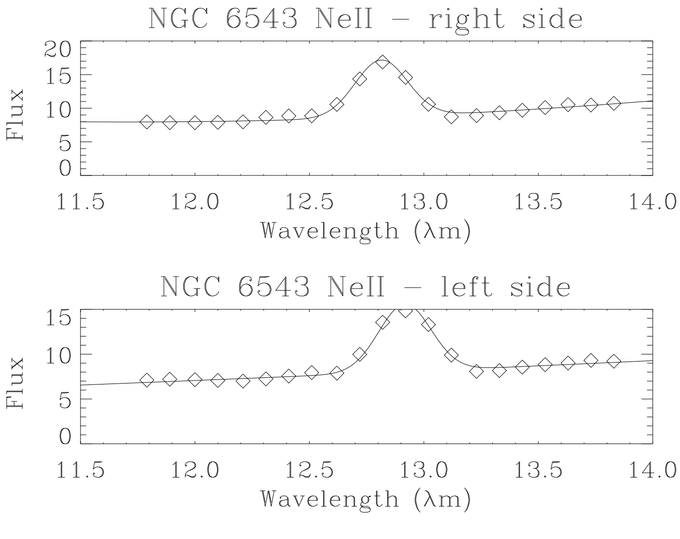

Figure 16: The spectrum of NGC 6543 around the NII line, as observed with the source put on the right side (top panel) and the left side (bottom panel) of the CAM detector. Flux units are arbitrary.

the total flux. Ghost images are difficult to disentangle from real images when the source is not point-like. A detailed optical model of the telescope and the CAM optics is needed to calibrate the size, shape, intensity and positions of the ghost images in the CVF. Such a model is in preparation (Okumura 1998b).

Additional problems come from straylight from sources outside the field-of-view. Using the 12″PFOV we have shown that regions of the detector outside the theoretical field-of-view are illuminated by straylight, that totals $\simeq$ 25 % of the flux within the region covered by the field mirror. Moreover we have shown that a flat-fielded image of the zodiacal background taken with the CVF is not flat, and deviations from flatness amount to $\sim$ 10 % on average. This limits the possibilities of imaging of faint extended sources with the CVF.

The CVF spectral calibration is very accurate when the source image is located at the centre of the array, but there is a systematic wavelength shift of up to +1 CVF step position, when the source image is located on the left of the CAM array. No shift is observed to the right of the detector. A more detailed calibration is needed in order to actually map this wavelength dependence for all CAM pixel positions, and at all wavelengths.

References

Abergel A., Désert F.-X., Aussel H. 1996, "IAS Model for ISOCAM LW Transient Correction", V.1.0
Blommaert J. 1997, "ISOCAM photometry report"
Cohen M., Witteborn F.C., Walker R.G., Bregman J.D., Wooden D.H. 1995, AJ 110, 275
Delaney M. 1997, "ISOCAM Interactive Analysis User's Manual", v.2.0
Lari C. 1997, "IRA model for ISOCAM LW transient correction"
Okumura K. 1998a, "ISOCAM PSF report"
Okumura K. 1998b, in preparation
Ott S. et al. 1996, "Design and implementation of CIA, the ISOCAM interactive analysis system", ASP Conference Series vol.125

List of abbreviations and symbols

- ADU, ADU/G, ADU/g - Analog to Digital Unit, the unit of all CAM observations, scaled by the gain factor;
- CVF - Circular Variable Filter;
- g, G - Gain;
- ICD - Internal Calibration Device;
- PFOV - Pixel Field-Of-View;
- PSF - Point Spread Function;
- s, sec - second, unit of time;
- T_{int} - the integration time of a single frame exposure;